Title

IL-1 Receptor–Knockout Mice Develop Epidermal Cysts and Show an Altered Innate Immune Response after Exposure to UVB Radiation

Journal

Journal of Investigative Dermatology, 137(11)

ISSN

0022-202X

Authors

Kulkarni, Nikhil N
Adase, Christopher A
Zhang, Ling-juan
et al.

Publication Date

2017-11-01

DOI

10.1016/j.jid.2017.07.814

Peer reviewed

HHS Public Access

Author manuscript

J Invest Dermatol. Author manuscript; available in PMC 2018 February 06.

Published in final edited form as:

J Invest Dermatol. 2017 November ; 137(11): 2417–2426. doi:10.1016/j.jid.2017.07.814.

IL-1 Receptor—Knockout Mice Develop Epidermal Cysts and Show an Altered Innate Immune Response after Exposure to UVB Radiation

Nikhil N. Kulkarni[1], **Christopher A. Adase**[1], **Ling-juan Zhang**[1], **Andrew W. Borkowski**[1], **Fengwu Li**[1], **James A. Sanford**[1], **Daniel J. Coleman**[2,3], **Carlos Aguilera**[1], **Arup K. Indra**[2,3,4,5,6,7], and **Richard L. Gallo**[1]

[1]Department of Dermatology, University of California, San Diego, California, USA

[2]Department of Pharmaceutical Sciences, College of Pharmacy, Oregon State University, Corvallis, Oregon, USA

[3]Molecular and Cellular Biology Program, Oregon State University, Corvallis, Oregon, USA

[4]Department of Biochemistry and Biophysics, Oregon State University, Corvallis, Oregon, USA

[5]Linus Pauling Science Center, Oregon State University, Corvallis, Oregon, USA

[6]Department of Dermatology, Oregon Health and Science University, Portland, Oregon, USA

[7]Knight Cancer Institute, Portland, Oregon, USA

Abstract

In this study, we observed that mice lacking the IL-1 receptor (IL-1R) (*IL1r*$^{-/-}$) or deficient in IL1-β developed multiple epidermal cysts after chronic UVB exposure. Cysts that developed in *IL1r*$^{-/-}$ mice were characterized by the presence of the hair follicle marker Sox 9, keratins 10 and 14, and normal melanocyte distribution and retinoid X receptor-α expression. The increased incidence of cysts in *IL1r*$^{-/-}$ mice was associated with less skin inflammation as characterized by decreased recruitment of macrophages, and their skin also maintained epidermal barrier function compared with wild-type mice. Transcriptional analysis of the skin of *IL1r*$^{-/-}$ mice after UVB exposure showed decreased gene expression of proinflammatory cytokines such as tumor necrosis factor-α and IL-6. In vitro, primary keratinocytes derived from *IL1r*$^{-/-}$ mice were more resistant to UVB-triggered cell death compared with wild-type cells, and tumor necrosis factor-α release was completely blocked in the absence of IL-1R. These observations illustrate an unexpected yet prominent phenotype associated with the lack of IL-1R signaling in mice and support further investigation into the role of IL-1 ligands in epidermal repair and innate immune response after damaging UVB exposure.

Correspondence: Richard L. Gallo, Department of Dermatology, University of California, San Diego, California 92093, USA. rgallo@ucsd.edu.

CONFLICT OF INTEREST

RLG is a consultant and has equity interest in MatriSys and Sente, Inc.

SUPPLEMENTARY MATERIAL

Supplementary material is linked to the online version of the paper at www.jidonline.org, and at http://dx.doi.org/10.1016/j.jid.2017.07.814.

INTRODUCTION

The IL-1 superfamily contains 21 proteins including 11 ligands and 10 receptors, co-receptors, or decoy receptors (Palomo et al., 2015). IL-1 cytokines can act as either agonists or antagonists of inflammation when bound to their respective receptor (Sims and Smith, 2010). IL-1 signaling can potentially affect all cells of the innate immune system because they either express or are directly or indirectly affected by IL-1 family members (Garlanda et al., 2013a). The balance between controlled immune response and uncontrolled inflammation via IL-1 signaling is tightly regulated through several mechanisms. These mechanisms include proteolytic activation of ligands by the inflammasome, receptor antagonists, decoy receptors, and negative regulators (Garlanda et al., 2013b; Palomo et al., 2015). Signaling via IL-1 cytokines can induce a secondary cascade of mediators affecting multiple cellular processes including chemotaxis, immunosuppression, and apoptosis (Nasti and Timares, 2012).

After insults like UVR exposure, the inflammasome complex including NALP3 is activated (Feldmeyer et al., 2007). This complex activates caspase 1, which proteolytically cleaves pro—IL-1β into its active form, IL-1β (Nasti and Timares, 2012), leading to activation of downstream proinflammatory signaling via NF-κB transcription factor and mitogen-activated protein kinases p38 and JNK and penultimately leading to secretion of proinflammatory proteins including tumor necrosis factor-α (TNF-α), IL-6, IL-1α, and IL-1β (Weber et al., 2010). IL-1 receptor (IL-1R) ligand IL-1β is known to play a key role in mediating signaling in autoinflammatory diseases through IL-1R (Dinarello, 2009). IL-1β is also well characterized for its role in immune response to infection (Netea et al., 2010). IL-1R ligands have more recently been shown to enhance chronic inflammation, leading to an increased expression of pro-tumorigenic factors (Apte et al., 2006; Cataisson et al., 2012; Kasza, 2013). IL-1R ligands have also been shown to influence hair growth in vitro (Harmon and Nevins, 1993; Hoffmann et al., 1997; Philpott et al., 1996) and in vivo (Groves et al., 1995). Polymorphisms in IL1RA or IL-1β are related to susceptibility and severity of the alopecia areata (Alfadhli and Nanda, 2014; Tarlow et al., 1994).

Given the role of UV damage in skin tumor development and the influence of IL-1 in inflammation, we sought to characterize the phenotype of mice exposed to UVB in the setting of abnormal IL-1 signaling. In this study, we report a striking phenotype in mice lacking IL-1R that become predisposed to form epidermal cysts after UVB damage and a general immunosuppression in these mice. These data show an unexpected role for IL-1R in epidermal homeostasis after injury.

RESULTS

Development of epidermal cysts in *IL1R*$^{-/-}$ and *IL1b*$^{-/-}$ mice exposed to chronic UVB

When damaged by UV exposure, keratinocytes produce IL-1 family proteins such as IL-1α and IL-1β (Nasti and Timares, 2012). To explore the relevance of this response in a chronic UV exposure protocol, we subjected wild-type (WT) and *IL1r*$^{-/-}$ mice to 200 mJ/cm^2 of UVB 3 times per week for 4 weeks, then 500 mJ/cm^2 of UVB 3 times per week for up to 150 days. An unexpected phenotype was observed in this experiment as *IL1r*$^{-/-}$ mice

developed multiple subcutaneous pigmented papules (Figure 1a, Supplementary Figure S1 online). Significantly fewer *IL1r*$^{-/-}$ mice (23%) were free of these lesions after 120 days of repeated UVB exposure compared with WT mice (94%) (see Supplementary Figure S1). No lesions were detected in either group in the absence of UVB treatment. To further explore the role of IL-1R ligands and inflammasomes, we next examined the response to chronic UVB irradiation in mice lacking IL-1β and the inflammasome component NLRP3. *IL1b*$^{-/-}$ mice showed increased papules but at a lower frequency compared with *IL1r*$^{-/-}$ mice, whereas *Nlrp3*$^{-/-}$ appeared similar to WT mice and did not show papule formation (Figure 1b, 1c). Next, we investigated the effect of chronic UVB response in mice lacking toll-like receptor (TLR) 3. Previous observation from our group showed that *Tlr3*$^{-/-}$ mice subjected to UVB irradiation have less skin inflammation than WT mice (Bernard et al., 2012);however, the rates of papule formation were similar between *Tlr3*$^{-/-}$ mice and WT mice (Figure 1d, 1e) after chronic UVB exposure.

Hematoxylin and eosin staining of dorsal skin after UVB exposure showed that the papules in *IL1r*$^{-/-}$ mice have a cystic structure (Figure 2a). The rare subcutaneous papules also detected in WT mice had a similar morphology to those in *IL1r*$^{-/-}$ mice (see Supplementary Figure S1c). No papillomas or carcinomas were detected under these treatment conditions.

Immunohistochemistry staining with the follicular marker Sox9 showed strong expression within the cysts. Most of the cells within the cysts were enucleated as indicated by negative staining for nuclear stain DAPI. Intermittent expression of epidermal differentiated cell marker keratin (K) 10 was observed, whereas only a few cells stained positive for the epidermal basal progenitor cell marker K14 (Figure 2b–d). No significant difference in the total melanocytes and retinoic X receptor (RXR)-α staining pattern was observed in the *IL1r*$^{-/-}$ mice skin compared with WT mice after chronic UVB irradiation (see Supplementary Figure S2a–c online).

IL1r$^{-/-}$ mice show a dampened immune response, less barrier disruption, and an altered transcriptional profile after UVB irradiation

IL1r$^{-/-}$ mice showed a decrease in infiltrating monocytes/macrophages (MAC1^{+} cells) in the dermal compartment compared with WT mice after UVB irradiation (Figure 3a, 3b). Furthermore, *IL1r*$^{-/-}$ mice had a significantly diminished increase in transepidermal water loss (TEWL) after acute UVB exposure than WT mice, indicating that WT mice had enhanced barrier disruption compared with the *IL1r*$^{-/-}$ mice (Figure 3c). To determine if the magnitude of the inflammatory response correlated with the change in barrier disruption, mice were pre-treated with cyclophosphamide, a known immunosuppressor (de Jonge et al., 2005; Huyan et al., 2011), before UVB exposure. Cyclophosphamide treatment alone had no effect on skin barrier function, but pretreatment with cyclophosphamide inhibited the increase in TEWL in WT mice after UVB (Figure 3d). These observations suggested that the lower TEWL in *IL1r*$^{-/-}$ mice after UVB exposure could be a result of the dampened inflammatory response.

To better understand how the lack of IL-1R promoted the development of cysts, we next looked at the changes in gene expression profile after an acute dose (up to 6 days) of UVB irradiation. RNA sequencing analysis of WT and *IL1r*$^{-/-}$ mice was performed on whole-skin

biopsy samples after an acute dose of UVB exposure. Hierarchical clustering of differentially expressed genes (3.8-fold) showed two distinct clusters, one for the WT (WT1 and WT2) and one for the *IL1r*$^{-/-}$ mice (IL1R-knockout 1 and IL1R-knockout 2) (Figure 4a). Analysis of the highly differentially regulated genes (4-fold change) for biological function through gene ontology enrichment analysis showed that several pathways related to cytoskeletal remodeling (keratin filament, cornified envelope, intermediate filament and keratinization) were up-regulated (Figure 4b) and that pathways related to chemotaxis and immune response were down-regulated (see Supplementary Figure S3b online). Network analysis was performed with the InnateDB database (Breuer et al., 2013) to understand the putative protein-protein interaction. The up-regulated protein-protein interaction showed interactions among cytoskeletal-associated proteins like Actn2, Ttn, Sptan1, and matrix metalloproteinases Mmp10 and Mmp7 (Figure 4c). These cytoskeletal-associated proteins, although indirectly, showed interaction with oncogenic pathway-related proteins such Hras and EGFR, neurotransmitters such as NOS1, and proteins related to calcium signaling (Calm1 and Camk2b). As a whole, this transcriptional profile was considered consistent with the phenotype observed in the *IL1r*$^{-/-}$ mice.

IL1r$^{-/-}$ mice are deficient in inflammatory gene expression after UVB exposure, whereas DNA damage response is not affected

Next, we validated changes in inflammatory cytokine/chemokine gene expression and compared this to expression of DNA repair genes in WT and *IL1r*$^{-/-}$ mice that were subjected to a short-term exposure protocol of three UVB exposures (200 mJ/cm^2 per exposure) with 48 hours between exposures (up to 6 days). Consistent with our prior results, acute UVB treatment of WT mice enhanced the expression of genes encoding inflammatory proteins TNF-α, IL-6, CXCL5, IL-1β and CCL2, whereas the expression of these genes was significantly lower in the *IL1r*$^{-/-}$ after UVB treatment (Figure 5 a–e).

The expression of genes encoding DNA damage repair-related proteins DDB2, ATM, and PARP1 was not affected after UVB treatment in either WT and *IL1r*$^{-/-}$ mice (Figure 5g–i). Similarly, immunohistological evaluation of phosphorylated γH2AX, a well-established marker for DNA damage, showed no difference in WT and *IL1r*$^{-/-}$ mice after UVB exposure (see Supplementary Figure S4a, S4b online). Normal human epidermal keratinocytes treated with IL-1β (2.5 ng/ml) and/or UVB treatment (30 mJ/cm^2) also showed no significant differences for expression of DNA damage repair-related genes and phosphorylated γH2AX (see Supplementary Figure S4c, S4d).

Next, because TNF-α cytokine release can promote a pro-apoptotic response (Barisic et al., 2008; Poppelmann et al., 2005), we examined whether epidermal keratinocytes (mKCs) isolated from *IL1r*$^{-/-}$ mice had abnormal TNF-α expression after treatment with UVB. mKCs were subjected to a single acute UVB dose (25 mJ/cm^2 or 30 mJ/cm^2) with measurements taken at increasing intervals (Figure 6). *IL1r*$^{-/-}$ mKCs had much less production of TNF-α, IP-10, and MIP-2 after UVB treatment (Figure 6a–c). The secretion of IL-1β and IL-6 was not affected after UVB treatment in WT and *IL1r*$^{-/-}$ mKCs (data not shown). Protein secretion of RANTES was not detected in mKCs. Next, we examined downstream signaling by immunoblotting against mitogen-activated protein kinase-

phosphorylated p38 and the apoptosis activation marker cleaved caspase 3, respectively (Figure 6d). WT mKCs showed a higher expression of phosphorylated p38 in UVB-irradiated WT cells than *IL1r*$^{-/-}$ mKCs. Endogenous levels of cleaved caspase 3 were lower in *IL1r*$^{-/-}$ mKCs than WT mKCs in nonirradiated cells, and a similar pattern was observed in UVB-treated cells (Figure 6d). Irradiating mKCs with UVB (25 mJ/cm^2) for 12 hours or 24 hours showed lower cell death in *IL1r*$^{-/-}$ than WT cells, as indicated by lesser rounded *IL1r*$^{-/-}$ mKCs compared with UVB-treated WT mKCs (Figure 6e). Quantification of cell viability by the CCK8 assay validated that *IL1r*$^{-/-}$ mKCs had less UVB-induced cell death (Figure 6f). mKCs from both WT and *IL1r*$^{-/-}$, treated with TNF-α (10 ng/ml or 40 ng/ml) showed significant and similar cell death response (Figure 6g). Taken together, these data suggest that UVB-mediated induction of TNF-α and associated secondary cell death is decreased in *IL1r*$^{-/-}$ mKCs.

DISCUSSION

UV exposure alters skin aging, pigmentation, immune responses, disease symptoms (i.e., rosacea, photodermatoses), and can lead to genomic instability affecting the likelihood of skin cancers (Grossman and Leffell, 1997; Marrot and Meunier, 2008; Wu et al., 2014). In this study, we observed that IL-1R–deficient mice (*IL1r*$^{-/-}$) form epidermal cysts when exposed to chronic UVB irradiation. Multiple cysts were seen in both IL1-β gene–deficient (*IL1β*$^{-/-}$) and *IL1r*$^{-/-}$ mice, but not in WT or *Nlrp3*$^{-/-}$ mice. The cysts observed in *IL1r*$^{-/-}$ mice stained positively for epithelial cell marker Sox9, were low in K14, and were enucleated, indicating that most of the cells within the cyst had undergone terminal differentiation. Indeed, gene ontology analysis showed that biological pathways related to cytoskeletal rearrangement and cornification were increased in *IL1r*$^{-/-}$ mice after UVB treatment. Overall, these observations are consistent with the phenotype that in the absence of IL-1R activation, there is a trend toward development of benign epidermal cysts after UV damage.

To understand why cysts formed more frequently after UV damage, we first sought to evaluate the role of inflammation. We have previously shown that UV-induced injury activates Tlr3-mediated proinflammatory responses (Bernard et al., 2012), and it has previously been suggested that activation of Tlr3 also enhances processing of pro–IL-1β via activation of caspase 8 (Maelfait et al., 2008). However, *Tlr3*-deficient (*Tlr3*$^{-/-}$) mice did not develop cysts at the same frequency as *IL1r*$^{-/-}$ mice, indicating that the specific disruption of IL-1R signaling, and not of an alternative proinflammatory pathway, is crucial for cyst formation. Indeed, *IL1β*$^{-/-}$ mice had a lesser extent of cyst formation compared with *IL1r*$^{-/-}$ mice.

Cysts produced by chronic UVB exposure had robust pigmentation. However, dorsal skin did not show significant changes in the total number or location of melanocytes between WT and *IL1r*$^{-/-}$ mice. Because RXRα is a key regulator involved in keratinocyte and/or melanocyte regulation, and cysts have been observed in mice with RXRα mutations (Li et al., 2000), it was also examined to determine if it was associated with cyst development in *IL1r*$^{-/-}$ mice. We observed no difference in RXRα expression pattern in *IL1r*$^{-/-}$ mice after UVB treatment compared with the WT mice.

Some prior reports have also suggested that IL-1 cytokines induce DNA damage and γH2AX phosphorylation (Cetkovic-Cvrlje and Eizirik, 1994; Davies et al., 2008; Oleson et al., 2014), although other reports suggest that IL-1 cytokines may be involved in triggering DNA damage repair via NF-κB and/or transforming growth factor-β signaling (Deorukhkar and Krishnan, 2010; Hubackova et al., 2012). In our study, no significant change was observed in DNA damage repair pathway-related gene expression and γH2AX phosphorylation between the *IL1r*$^{-/-}$ and WT mice exposed to UVB.

Finally, IL-1 signaling has been reported to enhance UVB-induced apoptosis through down-regulation of inhibitor of apoptosis proteins or increasing TNF-α cytokine release (Kothny-Wilkes et al., 1999) and also shifts TNF receptor 1 and NF-κB signaling to a pro-apoptotic pathway state (Barisic et al., 2008; Poppelmann et al., 2005). We therefore investigated whether IL-1R had a role in keratinocyte survival and TNF-α production. Keratinocytes isolated from *IL1r*$^{-/-}$ mice showed higher survival than WT cells after UVB treatment and also had significantly higher TNF-α production and downstream activation of phosphorylated p38 and cleaved caspase 3. These results suggest that under normal conditions, UVB injury triggers activation of the IL-1R signaling pathway that drives production and release of TNF-α, and this in turn stimulates secondary cell death. This response, combined with lesser inflammation, was the most significant association seen with the cyst phenotype. It needs to be established whether patients receiving IL-1R inhibitor therapy (e.g., anakinra) for treatment of inflammatory skin disorders have an increase in survival of DNA-damaged cutaneous cells because of suppressed apoptosis.

This study does not fully decipher the molecular mechanisms behind cyst formation, but it provides important new data that suggest biological pathways and candidate genes that are relevant for further investigation. To our knowledge there are no specific reports in the literature that UVB exposure promotes cyst formation in humans deficient in IL-1R or in patients receiving TNF-antagonist therapy, but this may be due to lack of sufficient observation. Thus, we present this description of a cyst-promoting environment in *IL1r*$^{-/-}$ mice as a new clue and potential model for further investigation into elements involved in epidermal homeostasis.

MATERIALS AND METHODS

Mice

Sex-matched C57BL/6 WT controls, male and female *IL1r*$^{-/-}$, IL-1β–deficient, and NLRP3-deficient and TLR3-deficient mice were all on a C57BL/6 background and were housed at the University Research Center at the University of California, San Diego. All animal experiments were approved by the University of California, San Diego Institutional Animal Care Committee.

UVB treatment

Mice were shaved and chemically depilated 3 days before beginning narrowband UVB irradiation (312 nm). UVB irradiation was performed using handheld UVB lamps from Spectronics (Westbury, NY) with two 8-W bulbs, as previously described (Borkowski et al.,

2015). For cyst formation experiments, 12-week-old mice were irradiated with 200 mJ/cm^2 UVB 3 times per week for 4 weeks and then with 500 mJ/cm^2 UVB 3 times per week for the remainder of the experiment. Dosimetry was performed using a digital UV radiometer from Solartech, Inc. (Parsippany, NJ). The 8-mm biopsy samples of the skin containing cysts were taken at the end of the experiment and used for histologic study. For measuring barrier disruption, mice were exposed to 50 mJ/cm^2 UVB. TEWL was measured using a TEWAMETER TM300 (C & K, Cologne, Germany). Mice treated with cyclophosphamide were given 300 mg/kg of cyclophosphamide intraperitoneally 48 hours before UVB exposure (50 mJ/cm^2). To measure relative changes in gene expression, mice were exposed to 300 mJ/cm^2 UVB and subsequently exposed to 200 mJ/cm^2 UVB every other day over the next 4 days. Punch biopsy samples were taken before initial UVB exposure and posttreatment days 1 and 6 after the initial UVB exposure. For RNA sequencing experiments, 12-week-old WT and *IL1r*$^{-/-}$ mice were shaved, and dorsal hair was chemically depilated. Twenty-four hours later, mice were exposed to 200 mJ/cm^2 narrowband UVB (312 nm) and subsequently exposed every other day over the next 4 days.

Murine keratinocyte isolation, normal human keratinocyte culture, UVB irradiation, and cell viability quantification

Primary adult mKCs were isolated from adult WT or *IL1r*$^{-/-}$ littermate mice as described previously (Zhang et al., 2012). Isolated mKCs and primary human adult keratinocytes (American Type Culture Collection) were cultured in EpiLife medium (Life Technologies, Waltham, MA) supplemented with 0.06 mmol/L $CaCl_2$ and EpiLife Defined Growth Supplement (Life Technologies) and penicillin-streptomycin (Life Technologies). After reaching approximately 90%, confluence the cells were treated with an acute dose of 25 mJ/cm^2 or 30 mJ/cm^2 UVB, as indicated in the figures. Cell viability was quantified by CCK-8 cell viability assay according to manufacturer's instructions (Dojindo Molecular Technologies, Rockville, MD).

Immunohistochemistry, histology, and image quantification

Skin samples for cyst characterization and MAC1 and RXRα staining were paraffinized and cut into 5-μm sections. Skin samples subjected to acute UVB irradiation were embedded in optimum cutting temperature compound (Tissue-Tek, Torrance, CA) and cut into 8-μm sections. Hematoxylin and eosin staining was performed after deparaffinization using xylenes and graded ethanol washes. Antigen retrieval for staining K10, Sox9, and K14 was performed in 1 mm EDTA (pH 8.0) and in citrate buffer (pH 6.0) for RXRα and MAC1 stainings for 20 minutes at 95°C in a water bath. After deparaffinization, antigen retrieval, and blocking, immunostaining was performed using primary antibodies recognizing K10 (Thermo Fisher Scientific, Waltham, MA; MS-611-P0; 1:50, mouse), K14 (Thermo Fisher Scientific; 1:100, rabbit), Sox-9 (Millipore, Billerica, MA; 1:100, rabbit), RXRα (Santa Cruz Biotechnology, Dallas, TX; 1:50, rabbit) and MAC1 (Abcam, Cambridge, UK; 1:1,000, mouse). γH2A.X-phosphorylated (Ser139) (Biolegend, San Diego, CA; 2F3, 1:200, mouse) was stained in optimal cutting temperature compound sections. For staining with primary antibodies raised in mice, M.O.M. Immunodetection kit (Vector Laboratories, Burlingame, CA) was used according to the manufacturer's instructions. Secondary antibodies used were Avidin-Alexa Fluor 488 (Thermo Fisher; 1:1,000) or Avidin-Alexa

Fluor 568 (Thermo Fisher; 1:500). For fluorescent immunohistochemistry, nuclei were counterstained with DAPI (200 ng/ml) for 10 minutes at room temperature. For chromogenic immunohisto-chemistry, sections were incubated with streptavidin-horseradish peroxidase (Vector Laboratories) for 30 minutes at room temperature and developed with DAB peroxidase substrate kit (Vector Laboratories). Slides were mounted with DPX mounting medium. Melanocytes were stained with the Fontana-Masson staining kit according to the manufacturer's instructions (American Master-Tech, Lodi, CA). Bright-field images were captured with a Leica DME light microscope using the Leica Application Suite software, version 3.3.1 (Leica, Wetzlar, Germany). Fluorescent images were captured using a Zeiss AXIO Imager.Z1 with a digital AxioCam HRm and processed using AxioVision 4.8 (Carl Zeiss, Oberkochen, Germany). Immunofluorescence quantification was performed by randomly choosing multiple fields and further processing with ImageJ software (National Institutes of Health, Bethesda, MD). Significance was determined using a two-tailed Student *t*-test.

RNA sequencing sample preparation and downstream analysis

Skin tissue was collected via punch biopsy, homogenized via beat beating in Trizol (Ambion, Waltham, MA) twice for 45 seconds, then RNA was isolated via an RNeasy kit (Qiagen, Hilden, Germany). RNA samples were then submitted to the University of California, San Diego Institute for Genomic Medicine for analysis by a Tapestation bioanalyzer (Agilent, La Jolla, CA). RNA sequencing was performed on a high-output run V4 platform (Illumina, San Diego, CA) in a single-read 100-cycle run. Subsequent analysis was done on Partek flow software (Partek, St. Louis, MO) using the Tophat2 aligner (version 2.0.8) quantifying to the transcriptome using the mm10_RefSeq Transcripts 16_08_01_v2. Hierarchal clustering used Euclidean distance and average pairwise linkage. Gene ontology enrichment analysis was performed on differentially regulated genes (≥2-fold and 4-fold, respectively) using Partek flow software. The protein-protein interaction network was generated in the InnateDB database (Breuer et al., 2013).

Quantitative real-time PCR

Tissues collected via punch biopsy were homogenized and processed with Direct-zol RNA isolation kit with DNase I treatment (Zymo Research, Irvine, CA). Cultured cells were lysed in Trizol, and RNA was extracted via Direct-zol kit (Zymoresearch, Irvine, CA). The isolated total RNA was quantified via nanodrop 2000/200c spectrophotometer (Thermo Fisher), and 1 μg of total RNA was used as a template to reverse-transcribe cDNA through an iScript cDNA Synthesis Kit (Bio-Rad, Hercules, CA). Pre-developed Taqman Gene Expression Assays (Life Technologies) were used to evaluate mRNA transcript levels of mouse or human genes. The expression of mouse genes *Tnfa, Il6, Cxcl5, Il1b, Ccl2, Ccl5, Ddb2, Atm, and Parp1* were evaluated. Mouse *Gapdh* was used as a reference gene. Similarly, human Taqman probes used were *OGG1, XPA, ATM, ATR, PARP1, APE1, PRKDC, DDB2, and IL6*. Human-specific *GAPDH* Taqman probe was used as a reference gene, as used in our previous study (Borkowski et al., 2015). The cDNA samples were analyzed in an ABI Prism 7000 Sequence Detection System (Life Technologies) and were performed in biological triplicates. The mRNA fold induction was calculated using the $\Delta\Delta C_t$ Livak method (Livak and Schmittgen, 2001). Results were significant at P less than 0.05.

The GraphPad prism software 5.0 (GraphPad, La Jolla, CA) was used for all statistical analysis.

Western blotting

The mKCs and normal human epidermal keratinocytes were lysed in radioimmunoprecipitation assay (i.e., RIPA) buffer after treatment, and total protein was quantified for each sample via bicinchoninic acid assay. Next, 5 μg of total protein was loaded onto a 4–20% Mini-PROTEAN TGX gel (Bio-Rad), transferred to a polyvinylidene difluoride membrane, and probed with primary antibodies against phosphorylated p38 (Cell Signaling, Danvers, MA; 1:100, rabbit), total p38 (Cell Signaling; 1:100, rabbit), cleaved caspase 3 (Cell Signaling; 1:500, rabbit), and phosphorylated-γH2AX (Abcam; 1:2,000, rabbit). Glyceraldehyde-3-phosphate dehydrogenase antibody (Abcam; 1:10,000, rabbit) was used as a loading control. Antirabbit secondary antibody conjugated to an infrared dye (IRDye800CW; Licor, Lincoln, NE) was used, and images were acquired on an Odyssey CLx imaging station (Licor).

ELISA and Luminex assays

Supernatant from mKCs was collected before RNA isolation, briefly centrifuged to remove debris, and stored at −80°C until further use. ELISA analysis was performed using a mouse TNF ELISA kit (BD OptEIA, BD Biosciences, San Jose, CA) following the manufacturer's instructions. IP-10, MIP-2, IL-1B, RANTES, and IL-6 were measured with a Milliplex MAP immunoassay kit (Millipore). The Milliplex assay was analyzed on MAGPIX platform (Luminex Corp., Austin, TX).

Supplementary Material

Refer to Web version on PubMed Central for supplementary material.

Acknowledgments

This work was supported in part by National Institutes of Health grants R01AR052728, R01AI052453, R01AR06781 (RLG), and R01 ES016629-01A1 (AKI); the UCSD Dermatologist Investigator Training Program T32AR062496 (AWB, CAA); and the National Cancer Institute of the National Institutes of Health award number T32CA106195.

Abbreviations

IL-1R	IL-1 receptor
K	keratin
mKC	mouse dermal kerati-nocyte
RXR	retinoic X receptor
TEWL	transepidermal water loss
TLR	toll-like receptor
TNF	tumor necrosis factor

WT wild type

References

Alfadhli S, Nanda A. Genetic analysis of interleukin-1 receptor antagonist and interleukin-1beta single-nucleotide polymorphisms C−511T and C+3953T in alopecia areata: susceptibility and severity association. Clin Exp Med. 2014; 14:197–202. [PubMed: 23584371]

Apte RN, Dotan S, Elkabets M, White MR, Reich E, Carmi Y, et al. The involvement of IL-1 in tumorigenesis, tumor invasiveness, metastasis and tumor-host interactions. Cancer Metastasis Rev. 2006; 25:387–408. [PubMed: 17043764]

Barisic S, Strozyk E, Peters N, Walczak H, Kulms D. Identification of PP2A as a crucial regulator of the NF-kappaB feedback loop: its inhibition by UVB turns NF-kappaB into a pro-apoptotic factor. Cell Death Differ. 2008; 15:1681–90. [PubMed: 18583989]

Bernard JJ, Cowing-Zitron C, Nakatsuji T, Muehleisen B, Muto J, Borkowski AW, et al. Ultraviolet radiation damages self noncoding RNA and is detected by TLR3. Nat Med. 2012; 18:1286–90. [PubMed: 22772463]

Borkowski AW, Kuo IH, Bernard JJ, Yoshida T, Williams MR, Hung NJ, et al. Toll-like receptor 3 activation is required for normal skin barrier repair following UV damage. J Invest Dermatol. 2015; 135:569–78. [PubMed: 25118157]

Breuer K, Foroushani AK, Laird MR, Chen C, Sribnaia A, Lo R, et al. InnateDB: systems biology of innate immunity and beyond—recent updates and continuing curation. Nucleic Acids Res. 2013; 41:D1228–33. database issue. [PubMed: 23180781]

Cataisson C, Salcedo R, Hakim S, Moffitt BA, Wright L, Yi M, et al. IL-1R-MyD88 signaling in keratinocyte transformation and carcinogenesis. J Exp Med. 2012; 209:1689–702. [PubMed: 22908325]

Cetkovic-Cvrlje M, Eizirik DL. TNF-alpha and IFN-gamma potentiate the deleterious effects of IL-1 beta on mouse pancreatic islets mainly via generation of nitric oxide. Cytokine. 1994; 6:399–406. [PubMed: 7948748]

Davies CM, Guilak F, Weinberg JB, Fermor B. Reactive nitrogen and oxygen species in interleukin-1-mediated DNA damage associated with osteoarthritis. Osteoarthritis Cartilage. 2008; 16:624–30. [PubMed: 17945515]

de Jonge ME, Huitema AD, Rodenhuis S, Beijnen JH. Clinical pharmacokinetics of cyclophosphamide. Clin Pharmacokinet. 2005; 44:1135–64. [PubMed: 16231966]

Deorukhkar A, Krishnan S. Targeting inflammatory pathways for tumor radiosensitization. Biochem Pharmacol. 2010; 80:1904–14. [PubMed: 20599771]

Dinarello CA. Interleukin-1beta and the autoinflammatory diseases. N Engl J Med. 2009; 360:2467–70. [PubMed: 19494224]

Feldmeyer L, Keller M, Niklaus G, Hohl D, Werner S, Beer HD. The inflammasome mediates UVB-induced activation and secretion of interleukin-1beta by keratinocytes. Curr Biol. 2007; 17:1140–5. [PubMed: 17600714]

Garlanda C, Dinarello CA, Mantovani A. The interleukin-1 family: back to the future. Immunity. 2013a; 39:1003–18. [PubMed: 24332029]

Garlanda C, Riva F, Bonavita E, Mantovani A. Negative regulatory receptors of the IL-1 family. Semin Immunol. 2013b; 25:408–15. [PubMed: 24239046]

Grossman D, Leffell DJ. The molecular basis of nonmelanoma skin cancer: new understanding. Arch Dermatol. 1997; 133:1263–70. [PubMed: 9382565]

Groves RW, Mizutani H, Kieffer JD, Kupper TS. Inflammatory skin disease in transgenic mice that express high levels of interleukin 1 alpha in basal epidermis. Proc Natl Acad Sci USA. 1995; 92:11874–8. [PubMed: 8524866]

Harmon CS, Nevins TD. IL-1 alpha inhibits human hair follicle growth and hair fiber production in whole-organ cultures. Lymphokine Cytokine Res. 1993; 12:197–203. [PubMed: 8218592]

Hoffmann R, Eicheler W, Wenzel E, Happle R. Interleukin-1beta-induced inhibition of hair growth in vitro is mediated by cyclic AMP. J Invest Dermatol. 1997; 108:40–2. [PubMed: 8980284]

Hubackova S, Krejcikova K, Bartek J, Hodny Z. IL1- and TGFbeta-Nox4 signaling, oxidative stress and DNA damage response are shared features of replicative, oncogene-induced, and drug-induced paracrine 'bystander senescence'. Aging. 2012; 4:932–51. [PubMed: 23385065]

Huyan XH, Lin YP, Gao T, Chen RY, Fan YM. Immunosuppressive effect of cyclophosphamide on white blood cells and lymphocyte subpopulations from peripheral blood of Balb/c mice. Int Immunopharmacol. 2011; 11:1293–7. [PubMed: 21530682]

Kasza A. IL-1 and EGF regulate expression of genes important in inflammation and cancer. Cytokine. 2013; 62:22–33. [PubMed: 23481102]

Kothny-Wilkes G, Kulms D, Luger TA, Kubin M, Schwarz T. Interleukin-1 protects transformed keratinocytes from tumor necrosis factor-related apoptosis-inducing ligand- and CD95-induced apoptosis but not from ultraviolet radiation-induced apoptosis. J Biol Chem. 1999; 274:28916–21. [PubMed: 10506136]

Li M, Indra AK, Warot X, Brocard J, Messaddeq N, Kato S, et al. Skin abnormalities generated by temporally controlled RXRalpha mutations in mouse epidermis. Nature. 2000; 407(6804):633–6. [PubMed: 11034212]

Livak KJ, Schmittgen TD. Analysis of relative gene expression data using realtime quantitative PCR and the 2(-Delta C(T)) Method. Methods. 2001; 25:402–8. [PubMed: 11846609]

Maelfait J, Vercammen E, Janssens S, Schotte P, Haegman M, Magez S, et al. Stimulation of Toll-like receptor 3 and 4 induces interleukin-1beta maturation by caspase-8. J Exp Med. 2008; 205:1967–73. [PubMed: 18725521]

Marrot L, Meunier JR. Skin DNA photodamage and its biological consequences. J Am Acad Dermatol. 2008; 58(5 Suppl 2):S139–48. [PubMed: 18410800]

Nasti TH, Timares L. Inflammasome activation of IL-1 family mediators in response to cutaneous photodamage. Photochem Photobiol. 2012; 88:1111–25. [PubMed: 22631445]

Netea MG, Simon A, van de Veerdonk F, Kullberg BJ, Van der Meer JW, Joosten LA. IL-1beta processing in host defense: beyond the inflammasomes. PLoS Pathog. 2010; 6(2):e1000661. [PubMed: 20195505]

Oleson BJ, Broniowska KA, Schreiber KH, Tarakanova VL, Corbett JA. Nitric oxide induces ataxia telangiectasia mutated (ATM) protein-dependent gammaH2AX protein formation in pancreatic beta cells. J Biol Chem. 2014; 289:11454–64. [PubMed: 24610783]

Palomo J, Dietrich D, Martin P, Palmer G, Gabay C. The interleukin (IL)-1 cytokine family—balance between agonists and antagonists in inflammatory diseases. Cytokine. 2015; 76:25–37. [PubMed: 26185894]

Philpott MP, Sanders DA, Bowen J, Kealey T. Effects of interleukins, colony-stimulating factor and tumour necrosis factor on human hair follicle growth in vitro: a possible role for interleukin-1 and tumour necrosis factor-alpha in alopecia areata. Br J Dermatol. 1996; 135:942–8. [PubMed: 8977716]

Poppelmann B, Klimmek K, Strozyk E, Voss R, Schwarz T, Kulms D. NF {kappa}B-dependent down-regulation of tumor necrosis factor receptor-associated proteins contributes to interleukin-1-mediated enhancement of ultraviolet B-induced apoptosis. J Biol Chem. 2005; 280:15635–43. [PubMed: 15723831]

Sims JE, Smith DE. The IL-1 family: regulators of immunity. Nat Rev Immunol. 2010; 10:89–102. [PubMed: 20081871]

Tarlow JK, Clay FE, Cork MJ, Blakemore AI, McDonagh AJ, Messenger AG, et al. Severity of alopecia areata is associated with a polymorphism in the interleukin-1 receptor antagonist gene. J Invest Dermatol. 1994; 103:387–90. [PubMed: 8077705]

Weber A, Wasiliew P, Kracht M. Interleukin-1 (IL-1) pathway. Sci Signal. 2010; 3(105):cm1. [PubMed: 20086235]

Wu S, Han J, Laden F, Qureshi AA. Long-term ultraviolet flux, other potential risk factors, and skin cancer risk: a cohort study. Cancer Epidemiol Biomarkers Prev. 2014; 23:1080–9. [PubMed: 24876226]

Zhang LJ, Bhattacharya S, Leid M, Ganguli-Indra G, Indra AK. Ctip2 is a dynamic regulator of epidermal proliferation and differentiation by integrating EGFR and Notch signaling. J Cell Sci. 2012; 125(Pt. 23):5733–44. [PubMed: 23015591]

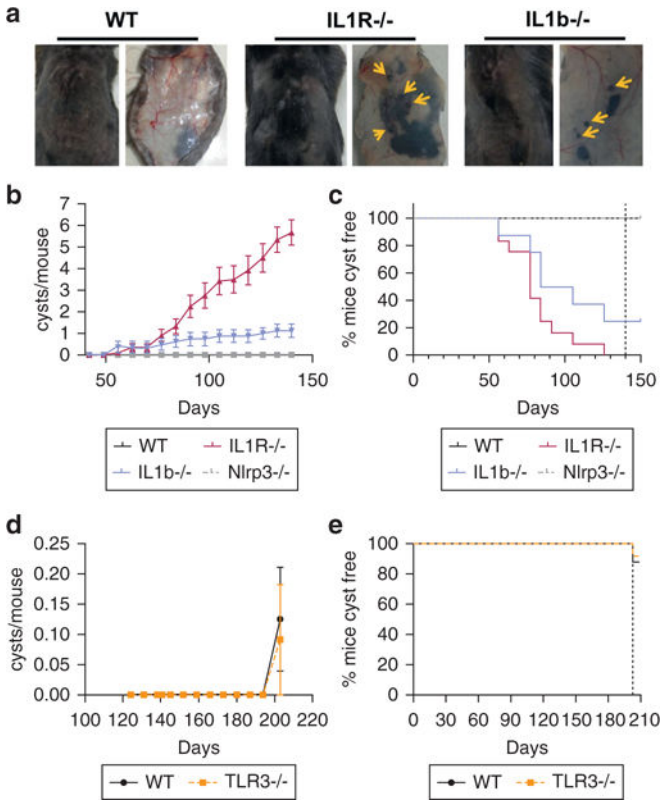

Figure 1. $IL1r^{-/-}$ and $IL1\beta^{-/-}$ mice develop papules after chronic exposure to UVB radiation

(**a**) Papules are shown with arrows on the external view of dorsal skin (left image) and dermal view of skin after removal of WT mice compared with $IL1r^{-/-}$ and $IL1b^{-/-}$ mice after 150 days of chronic UVB irradiation. (**b**) Average number of papules (cysts) per mouse detected on WT (n =1 0), $Nlrp3^{-/-}$ (n = 8), $IL1r^{-/-}$ (n = 12), and $IL1b^{-/-}$ (n = 8) mice. (**c**) Fraction of mice from **b** that did not have detectable cysts. (**d**) Average number of papules detected on WT mice (n = 10) or $Tlr3^{-/-}$ mice (n = 12) after 200 days of chronic UVB irradiation. (**e**) Fraction of mice from **d** that did not have detectable cysts. IL-1R, IL-1 receptor; TLR, toll-like receptor; WT, wild type.

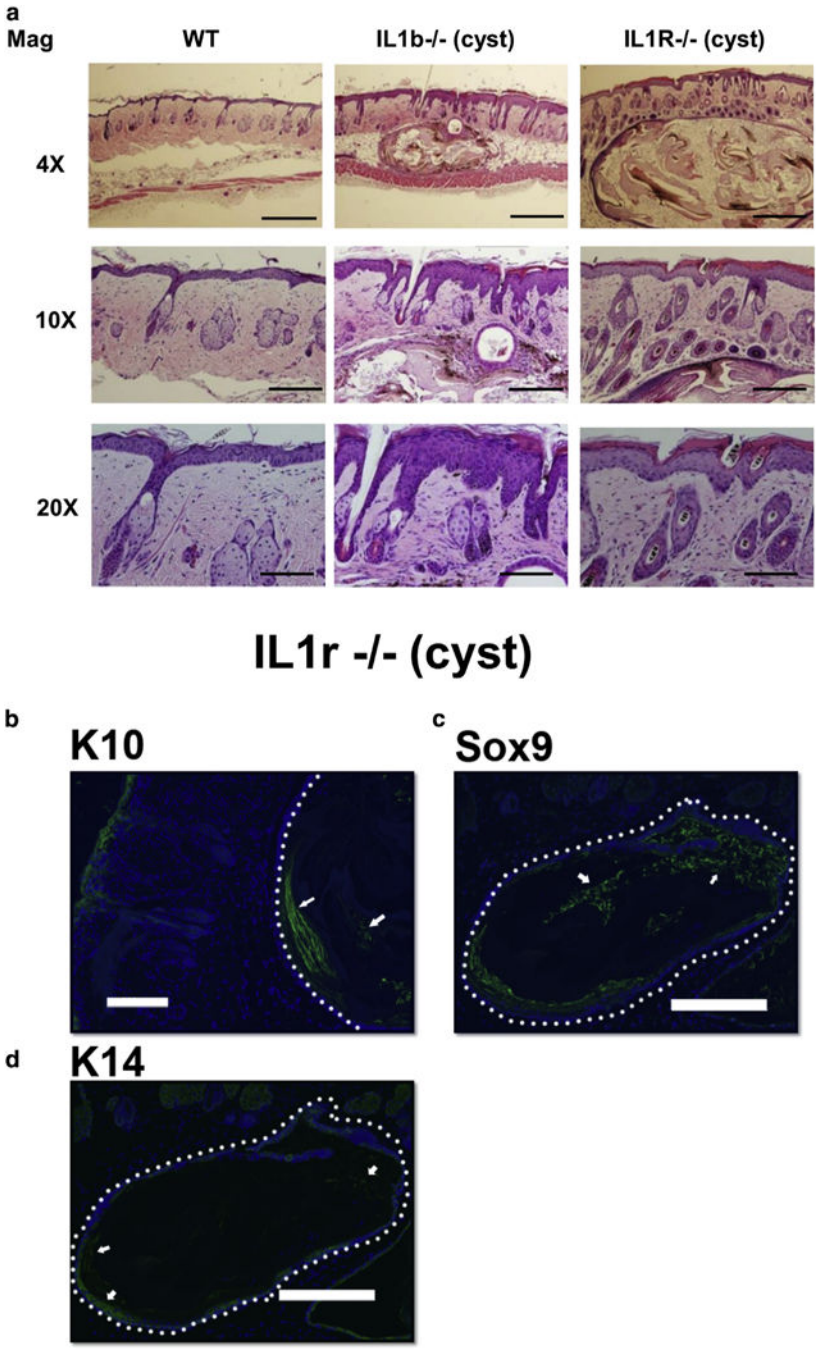

Figure 2. UVB radiation promotes cysts in *IL1b*$^{-/-}$ and *IL1r*$^{-/-}$ mice

(**a**) Representative image of WT, *IL1b*$^{-/-}$, and *IL1r*$^{-/-}$ mouse dorsal skin after 180 days of UVB exposure stained with hematoxylin and eosin. For 4×, scale bar = 500 μm; 10×, scale bar = 200 μm; 20×, scale bar = 100 μm. (**b–d**) Immunofluorescence staining of cysts found in *IL1r*$^{-/-}$ mice with differentiated dermal cell marker K10, follicular cell marker Sox9, and basal cell marker K14. Nuclei are counterstained with DAPI (blue). White dotted line is used to demarcate cysts. White arrows indicate positive staining within the cysts. Scale bar = 200 μm. IL-1R, IL-1 receptor; K, keratin; Mag, magnification on images; WT, wild type.

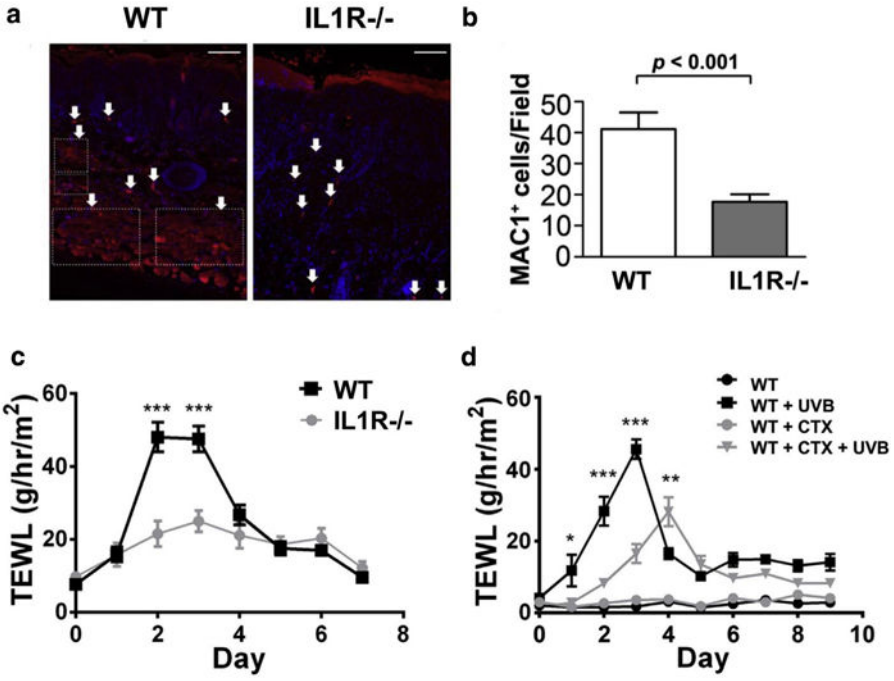

Figure 3. *IL1r*$^{-/-}$ mice show decreased recruitment of macrophages and decreased TEWL disruption after UVB exposure

(**a**) Dorsal skin of WTand *IL1r*$^{-/-}$ mice were stained for infiltrating monocytes/macrophages using the MAC1 primary antibody (red) and counterstained with DAPI (blue). Scale bar = 50 μm (**b**) MAC1-positive cells from **a** were quantified by Image J software and are represented as MAC1^{+} cells/field. *P*-value represents Student *t*-test. Marked boxes indicate migrated macrophage population. Arrows indicate positive staining for MAC1. (**c**) TEWL measured daily for 7 days after exposure to a single dose of 50 mJ/cm^2 UVB, WT (n = 6) or *IL1r*$^{-/-}$ mice (n = 6). (**d**) WT control (n = 10) or WT mice pre-injected with the immune system suppressor drug cyclophosphamide (CTX) (n = 10) were exposed to an acute dose of 50 mJ/cm^2 UVB. TEWL was measured over 7 days. **P*< 0.05, ***P*< 0.01, ****P*< 0.001. IL-1 R, IL-1 receptor; TEWL, transepidermal water loss; WT, wild type.

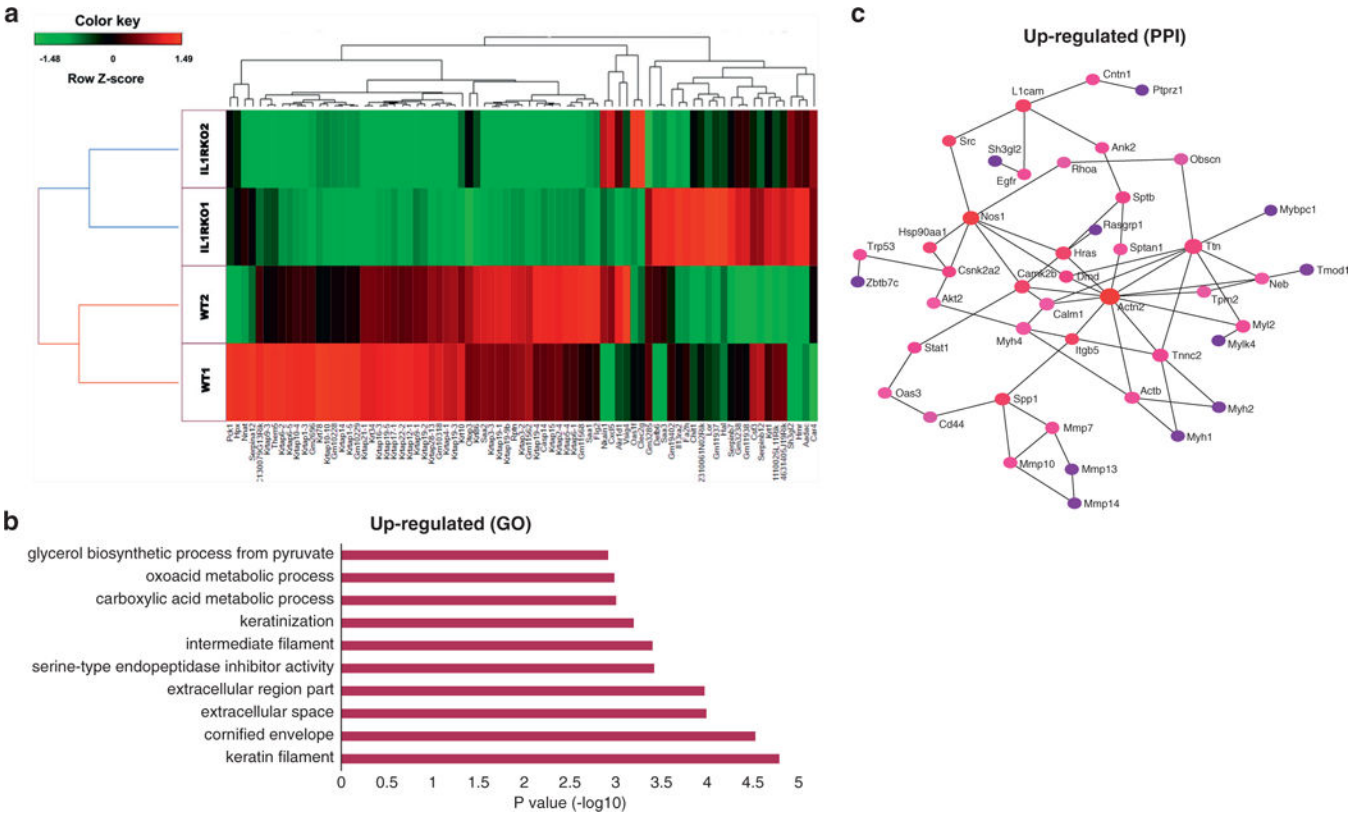

Figure 4. ***IL1r*$^{-/-}$ mice have altered transcriptional profile after UVB exposure**

(**a**) Heatmap and hierarchical clustering of RNA sequencing gene expression profile (3.8-fold change) from WT (n = 2) and *IL1r*$^{-/-}$ (n = 2) mice after a 6-day acute UVB exposure (200 mJ/cm^2 dose, 1 dose every 48 hours, 3 doses in total). (**b**) Top 10 hits of gene ontologies (GO) of the significantly up-regulated (≥4-fold) genes are represented. (**c**) Protein-protein interaction (PPI) networks were derived from network analysis in InnateDB. The putative PPIs from the up-regulated (≥2-fold) genes are represented. The color of nodes represents their betweenness centrality values. Red and blue colors indicate highest and lowest betweenness centralities, respectively.

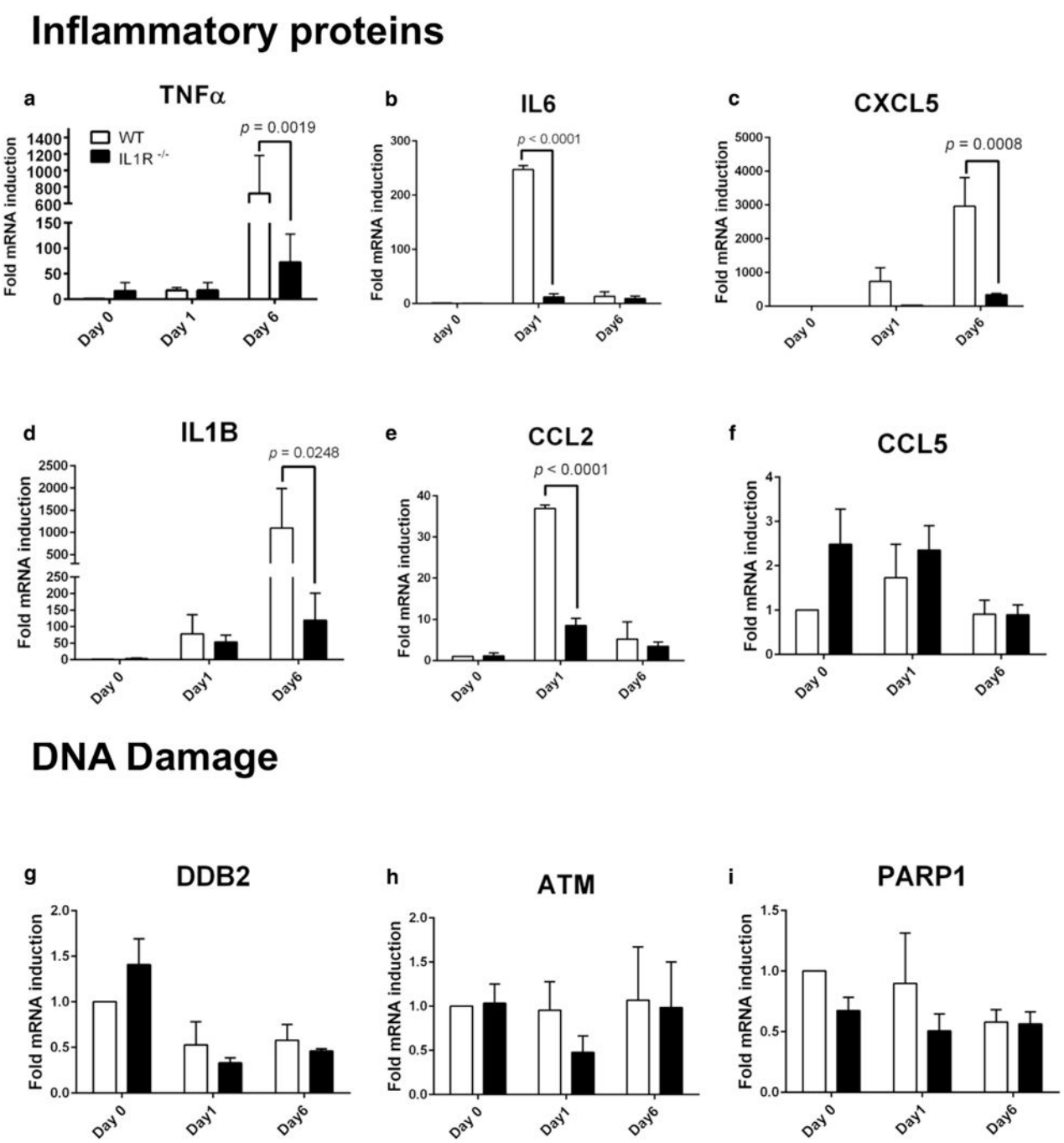

Figure 5. Validation of mRNA expression in skin of *IL1r*$^{-/-}$ mice after UVB exposure

Quantitative real-time reverse transcriptase–PCR quantification of expression of the genes encoding (**a**) TNF-α, (**b**) IL6, (**c**) CXCL5, (**d**) IL1B, (**e**) CCL2, (**f**) RANTES (*CCL5*), (**g**) DDB2, (**h**) ATM, and (**i**) PARP1 from dorsal skin tissue punch biopsy samples of WT (n = 4) or *IL1r*$^{-/-}$ (n = 4) mice at baseline (day 0), 24 hours after a single dose of UVB irradiation (300 mJ/cm^2) (day 1), or 24 hours three doses of UVB irradiation (300 mJ/cm^2) (day 6). IL-1R, IL-1 receptor; TNF, tumor necrosis factor; WT, wild type.

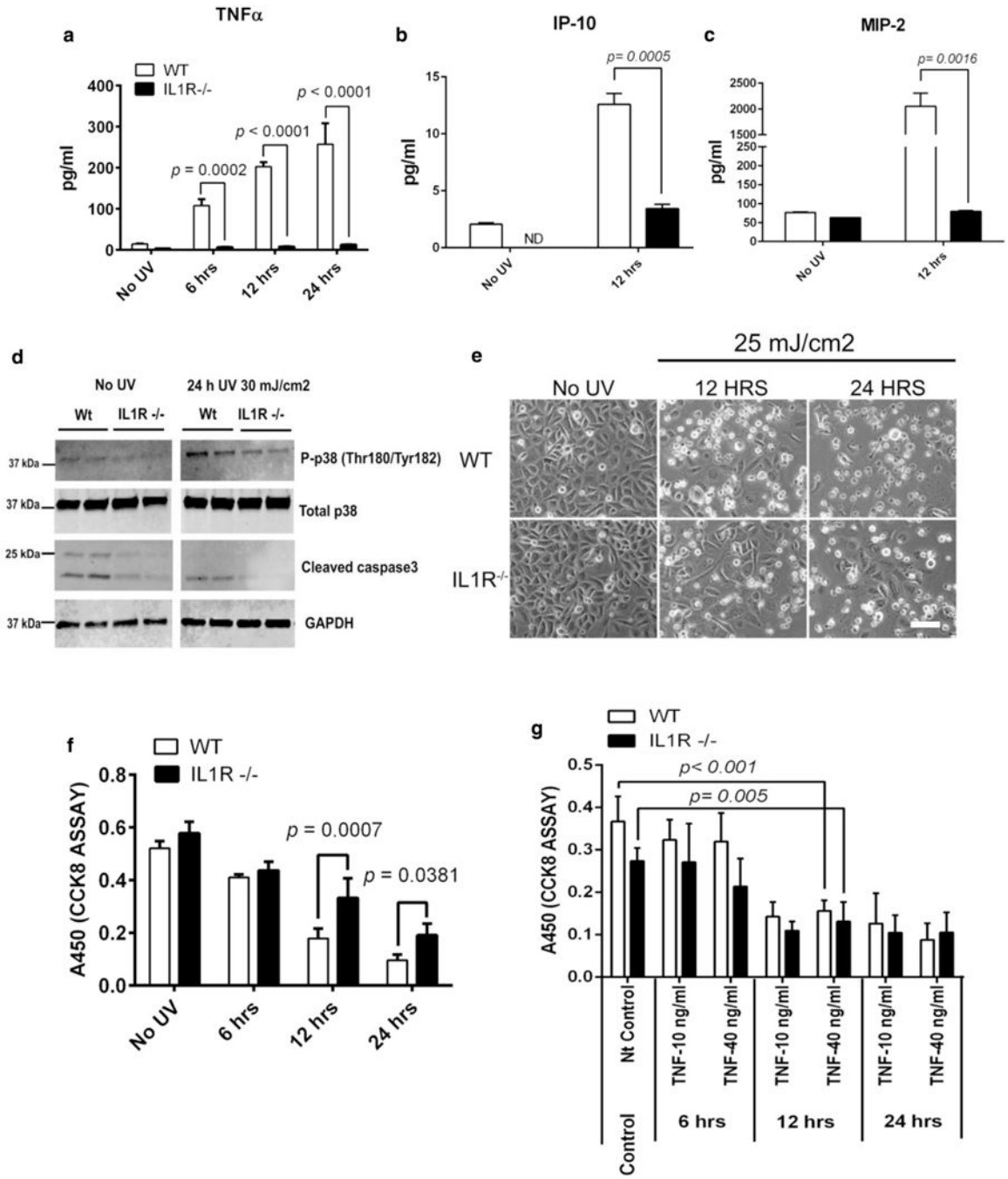

Figure 6. Keratinocytes from *IL1r*$^{-/-}$ mice show lower inflammatory protein secretion compared with WT mice after acute UVB exposure and are more resistant to UVB-induced cell death

(**a**) UVB (30 mJ/cm^2)-induced release of TNF-α by primary adult mouse keratinocytes (mKCs) was measured by a sandwich ELISA at indicated time points. (**b, c**) Similarly, IP-10and MIP-2 secretion was measured after 12 hours UVB (30 mJ/cm^2) treatment by Milliplex assay. (**d**) Activation of mitogen- activated protein kinase p38and apoptosis were looked at by immunoblotting against phosphorylated p38 (P-p38) and cleaved caspase 3, respectively. Total p38 and GAPDH were used as loading controls. (**e**) mKCs were isolated

from WTor *IL1r*$^{-/-}$ skin and cultured to approximately 90% confluence before exposure to UVB (25 mJ/cm^2). Phase contrast images were taken at 12 hours and 24 hours after UVB exposure. Scale bar = 50 μm. (**f**) Cell viability of keratinocytes from WT and *IL1r*$^{-/-}$ was quantified by CCK-8 cell viability assay at 6 hours, 12 hours, and 24 hours after UVB treatment (30 mJ/cm^2). (**g**)WT and *IL1R*$^{-/-}$ mice were treated with TNF-α (10 ng/ml or 40 ng/ml) for 6 hours, 12 hours, and 24 hours, and cell death was measured by CCK8 assay. *P*-values were calculated by one-way analysis of variance multiple comparison test. GAPDH, glyceraldehyde-3-phosphate dehydrogenase; h, hour; hrs, hours; IL-1R, IL-1 receptor; Nt control, nontreated control; TNF, tumor necrosis factor; WT, wild type.